

1 **Experimental study of directional detection of neutrons and gamma rays using**
 2 **an elpasolite scintillator array**

3 A. Guckes ^{a,*}, A. Barzilov ^b, P. Guss ^c

4 ^a *Nevada National Security Site, North Las Vegas Operations, P.O. Box 98521, M/S NVL-068, Las Vegas, Nevada 89193-8521, USA, guckesal @nv.doe.gov, 1-702-295-0199*

5 ^b *University of Nevada Las Vegas, 4505 S. Maryland Parkway, Las Vegas, NV 89154, USA*

6 ^c *Nevada National Security Site, Remote Sensing Laboratory - Nellis, P.O. Box 98521, M/S RSL-09, Las Vegas, NV 89193-8521, USA*

7 ^{*}Corresponding author

8 **Highlights**

9 • Detection system based on elpasolite CLYC scintillators was studied for directional detection of neutrons and
 10 gamma rays.
 11 • Experimental study of the scintillator responses was carried out using a three-cell array.
 12 • Maximum likelihood estimation technique was used to localize a radiation source.
 13 • Three-cell array is feasible to ascertain the direction to a neutron source and a gamma-ray source.

14 **Abstract**

15 A radiation detection system consisting of an array of three $\text{Cs}_2\text{LiYCl}_6:\text{Ce}^{3+}$ elpasolite cells was studied for
 16 simultaneous, directional neutron and gamma-ray measurements. Utilizing a neutron source and gamma-ray
 17 sources, measurements were carried out while rotating the three-cell array 360° . The measurement data were
 18 processed using a maximum likelihood estimation technique to determine the most probable angle pointing to the
 19 radioactive source. The detection system enables measuring gamma rays and neutrons simultaneously and
 20 estimating locations of radioactive sources within 23° .

21 **Keywords:** Elpasolite scintillator; CLYC; directional detector; neutron measurements; gamma spectroscopy.

22 **1. Introduction**

23 Radiation measurement systems are important to preventing nuclear weapons proliferation and supporting
 24 homeland security tasks such as detection, quantification and tracing of radioactive sources including nuclear
 25 materials [1-4]. Radiological and nuclear materials can be smuggled into countries through seaports and border
 26 crossings [5]. Radioactive sources have been stolen or lost exposing the public to elevated levels of radiation [6].
 27 Radioactive isotopes can be discharged into the environment because of natural catastrophes or accidents at
 28 facilities such as the disaster at the Fukushima Daichi nuclear power plant [7-10]. In remote monitoring, photon
 29 and neutron measurements are utilized because charged particles such as electrons and alpha particles are
 30 attenuated by a thin shielding layer and have short ranges in air. Gamma and neutron detection are essential for
 31 nuclear waste management and environmental safety [11, 12], active material assay technologies [13-15], and dual-
 32 particle imaging techniques [16, 17]. It is imperative to continue to advance gamma and neutron detection
 33 capabilities to prevent and mitigate growing radiological and nuclear threats and support radiation measurement
 34 technologies for applications in different areas.

35 One such advancement in radiation detection is the ability to simultaneously detect neutrons and gamma rays
 36 using a single detector. Previously, two separate detection systems were employed: one system for the gamma
 37 spectroscopy, and another system for neutron counting. For example, a high purity germanium detector with
 38 cryocooling or a sodium iodide scintillator was used to measure a gamma spectrum, and a ^3He tube equipped with

50 a moderator was employed for neutron measurements [18]. The use of two different detectors with coupled
51 electronics, power supplies, and software makes the gamma/neutron sensing system complex, bulky, and costly.
52 Therefore, a dual mode (gamma rays and neutrons) detection system, preferably an ambient temperature design,
53 is necessary especially for deployment in field conditions. Liquid and plastic scintillators enable detecting both
54 photons and neutrons by a single sensor; however, their energy resolution is poor for the gamma spectroscopy [19-
55 21].

56 The elpasolite scintillator $\text{Cs}_2\text{LiYCl}_6:\text{Ce}^{3+}$ (CLYC) allows gamma and neutron detection with no cryogenic
57 cooling needed [22-24]. CLYC's density is 3.31 g/cm³. The refractive index is 1.81 at 405 nm. CLYC is a bright
58 scintillator; its outputs are 20,000 photons per one absorbed 1-MeV gamma ray and 70,000 photons per one
59 absorbed thermal neutron. Gamma rays interact with the CLYC primarily by means of Compton scattering,
60 photoelectric absorption, and pair production. The full width at half maximum (FWHM) energy resolution for 662
61 keV gamma rays is less than 5%. Neutron detection is achieved via ${}^6\text{Li}(n,\alpha)t$ reaction (the cross-section is 940
62 barns). The α -particle and ${}^3\text{He}$ ion share energy of 4.78 MeV, generating ionization tracks in CLYC. The trapping
63 of free charges in Ce^{3+} scintillation centers leads to the de-excitation with production of a light pulse. In the energy
64 spectrum, the associated peak is recorded at 3.0 MeV gamma-equivalent energy (GEE) with the FWHM energy
65 resolution of 3%. It enables pulse height discrimination of neutron and photon events, except the 3-MeVee peak
66 width region. In addition to the detection of gamma rays and thermal neutrons, fast neutron detection using CLYC
67 is feasible via (n,p) reaction on ${}^{35}\text{Cl}$ isotope leading to production of ${}^{35}\text{S}$ [25, 26]. The Q -value of this reaction is
68 0.615 MeV; the emitted proton's energy is the incident neutron energy plus the Q -value. The resultant peak appears
69 at a GEE proportional to the incident neutron energy. Thus, fast-neutron spectroscopy is possible with CLYC
70 although it was not exploited in this study.

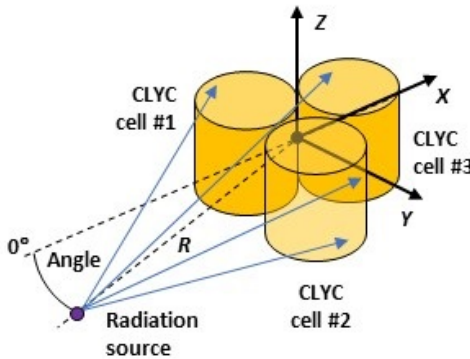
71 The CLYC scintillation emission includes three distinct decay components [27, 28]. Two components appear
72 due to gamma ray interactions with the CLYC scintillator and include the core-to-valence luminescence (CVL)
73 [29] and prompt Ce^{3+} emission. The CVL has 250 nm – 350 nm wavelength range and 2 ns decay time constant.
74 The Ce^{3+} emission wavelength range is 350 nm – 450 nm, and the decay time constant is 50 ns. The third
75 component that appears due to a neutron interaction within the CLYC is cerium self-trapped excitation (Ce-STE).
76 It has 350 nm – 450 nm range and 1,000 ns decay time constant. The substantial difference in the decay times of
77 the gamma-ray induced versus neutron-induced emission components of CLYC allows for an excellent pulse shape
78 discrimination (PSD) between neutrons and gamma rays [30, 31]. To increase thermal neutron detection efficiency,
79 the ${}^6\text{Li}$ -enriched CLYC crystals were grown. For example, the 95% ${}^6\text{Li}$ enriched CLYC (or CLYC6 material)
80 enabled 2.3 times larger thermal neutron cross section compared to the cross section of ${}^3\text{He}$ gas of the same volume
81 at 9.86 atmospheres [32].

82 Directional gamma and neutron detection systems that make it possible to locate positions of the sources are
83 often needed [33-37]. Elpasolite detectors can be used for directional detection of photons and neutrons [38, 39].
84 Computational studies showed that a directional detection system consisting of an array of elpasolite detectors is
85 feasible for simultaneous measurements of neutron and photon flux with the localization of radiation sources [40].
86 A detection system consisting of an array of three CLYC6 cells was developed and utilized in this study to
87 experimentally ascertain the feasibility of such a system to address the directional sensing of gamma rays and
88 neutrons simultaneously. Gamma spectroscopy, neutron/gamma PSD, and radiation source localization were
89 performed. The experimental setup and test results are discussed herein.

90 2. Directional neutron and photon measurements

91 2.1 Experimental setup

92 An array of three cylindrical CLYC6 scintillator cells was developed. The array consisted of two 1-inch
93 diameter by 1-inch height scintillators (denoted as CLYC #1 and CLYC #2) and one 1.5-inch diameter by 1.5-inch
94 height CLYC scintillator (denoted as CLYC #3). The scheme of the three-cell array arranged as a symmetrical,
95 tightly packed assembly is shown in Fig. 1. Elpasolite scintillator cells in this arrangement shadow each other
96 partially blocking an incident photon or neutron at different angles. Therefore, incident gamma rays and neutrons



100
101
102 **Figure 1.** Scheme of the directional detection system.
103

104 generate different responses in the CLYC6 cells at different angles. This information enables deducing the angle
105 pointing to the emitting source.

106 CLYC6 scintillators used in this study were procured from Radiation Monitoring Devices. To characterize each
107 cell, neutron/gamma PSD and gamma spectroscopy measurements were carried out using a bialkali Hamamatsu
108 R6231-100-01HA photomultiplier tube (PMT) matching the scintillation emission range of CLYC, high voltage
109 (HV) base and a single-channel eMorpho digitizer (Bridgeport Instruments). The analog signals of the PMT anode
110 were digitized. Then, the digital waveforms were analyzed yielding the following three parameters in a list mode:
111 a waveform's start time, an integral under the waveform that is related to the energy of radiation absorbed in the
112 CLYC cell, and 'partial' integral calculated only under the front portion of the signal based on the preset time
113 window. These list-mode parameters were used for the neutron/gamma PSD analysis utilizing a radiation
114 identification (RID) value calculated as a ratio of integrals under the tail portion and front portion of the waveform.
115 Because neutron-induced waveforms exhibit longer tail parts than photon-induced waveforms, and similar rise
116 times, the 'neutron' RID values are greater. It allows separating neutron events and photon events based on RIDs.
117

118 This study was performed at the nuclear engineering laboratory of University of Nevada Las Vegas. The
119 laboratory houses a shielded vault containing radioactive sources: a moderated 2-Curie $^{239}\text{PuBe}$ source, 0.898- μCi
 ^{137}Cs and a 0.9314- μCi ^{60}Co gamma check sources. Separated photon list-mode data were used to generate the
120 gamma energy spectrum. The spectrum was calibrated using gamma test sources. The FWHM energy resolution
121 of the 662 keV peak for ^{137}Cs and 1.17 MeV and 1.33 MeV peaks for ^{60}Co were determined employing a Gaussian
122 fit.

123 The source localization measurements were performed with an array of three CLYC scintillators each with its
124 own PMT and HV base. All three detectors were mounted on to a rotating turntable. Direction indicators were
125 placed at each 10° increment through 360° on the turntable. A four-channel qMorpho MCA/digitizer (Bridgeport
126 Instruments) was used to analyze signals of three CLYC cells. Both digitizers were linked via USB to a PC running
127 the Igor Pro user interface providing communication between the user and the detection system and processing
128 capabilities to analyze the measured radiation data.

129
130 *2.2 Source localization*
131

132 For source localization measurements, the detector system was set atop a turntable that provided 360°
133 rotation of the system in the xy -plane. For gamma measurements only, a source holder was used to move the
134 source being detected along the z -axis (vertically) to provide a third dimension to the source location. The
135 $^{239}\text{PuBe}$ source was too heavy to move along the z -axis. However, three-dimensional measurements of the
136 gamma-ray sources are representative of how the detector system would respond to a source in the field that is
137 not in the plane of the detection system.

138 For each source placement scenario, the detector system was rotated 360° in the xy -plane in increments of 40°.
 139 Data gathered from each detector in the three-cell array at each angle was processed using a maximum likelihood
 140 estimation (MLE) procedure. The MLE methodology is a statistical analysis that provides means to estimate
 141 unknown parameters for a set of data [41]. In this study, it is the angle pointing to a radioactive source location
 142 that was estimated using MLE. The angular dependent data measured by each CLYC cell in the three-cell array
 143 was fitted with a sum of sine model. The angle at which each fitted function has a maximum is the most probable
 144 source angle for that specific cell assuming that each detector will observe the maximum number of counts when
 145 the greatest amount of each detector's surface area is exposed to the radiation emitted from the source. It was also
 146 assumed that the observed source direction obtained from each detector in the array is normally distributed with
 147 the probability density function (PDF):
 148

$$P(\varphi_m | \theta, \sigma^2) = \frac{1}{\sqrt{2\pi}\sigma} \exp \frac{-(\varphi_m - \theta)^2}{2\sigma^2} \quad (1)$$

149 where φ_m is the observed source angle from the measured data for the m -th detector, θ is the actual source angle
 150 (unknown), and σ^2 is the variance of θ . Since all cells are independent, the PDF for the angle pointing to the source
 151 considering all three cells in the array is:

$$P(\{\varphi_m\}_{m=1}^3 | \theta, \sigma^2) = \prod_{m=1}^3 P(\varphi_m | \theta, \sigma^2) \quad (2)$$

152 The likelihood function of Eq. 2 is defined as:

$$Lf(\theta, \sigma^2) = \ln[P(\{\varphi_m\}_{m=1}^3 | \theta, \sigma^2)] \quad (3)$$

153 The maximum likelihood estimate for the source angle is a θ value that maximizes the likelihood function:

$$\hat{\theta} = \arg \max_{\theta} Lf(\theta, \sigma^2) \quad (4)$$

154 The variance of $\hat{\theta}$ is defined as:

$$\hat{\sigma}^2 = \frac{1}{3} \sum_{m=1}^3 (\varphi_m - \hat{\theta})^2 \quad (5)$$

155 The standard deviation can be deduced from the variance. The angle from the detector system to the neutron
 156 or gamma-ray source being evaluated was known in this study. However, if this system would be deployed in the
 157 field to find a lost, stolen, or smuggled radioactive source or nuclear material, the exact position of the source will
 158 not be known prior to the measurements. By comparing the MLE evaluated angle to the actual angle representing
 159 the course location, it can be determined how well this detector system would find a radioactive source of unknown
 160 location in the field.

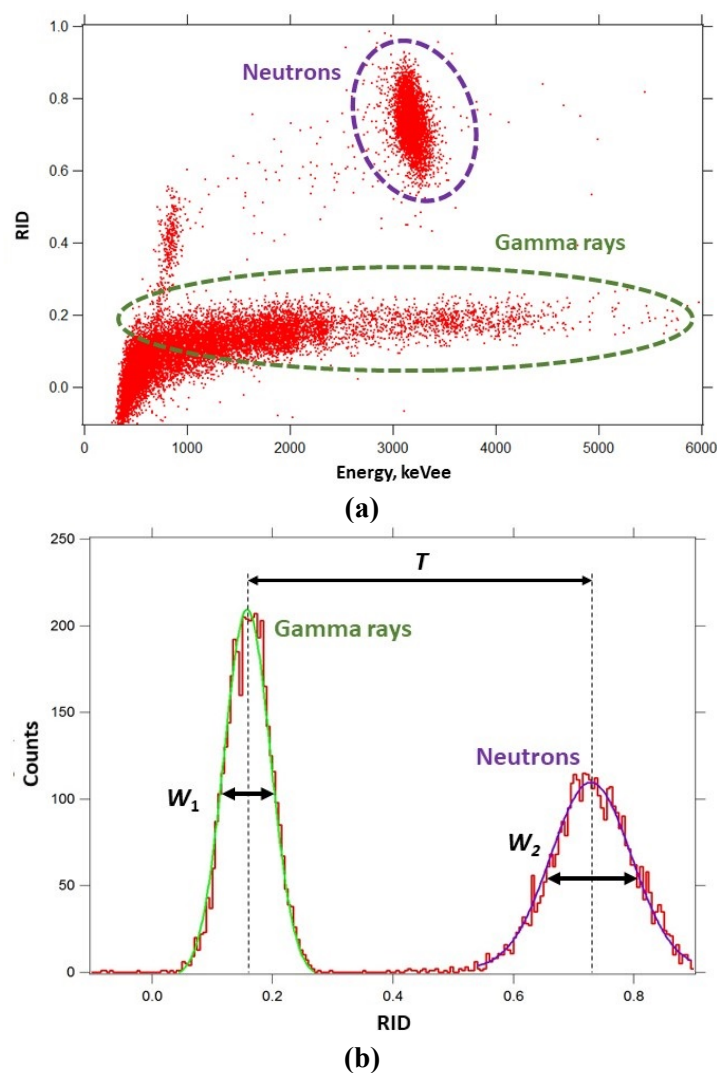
161

162

163

164 **3. Results and discussion**165 **3.1 Pulse shape discrimination**

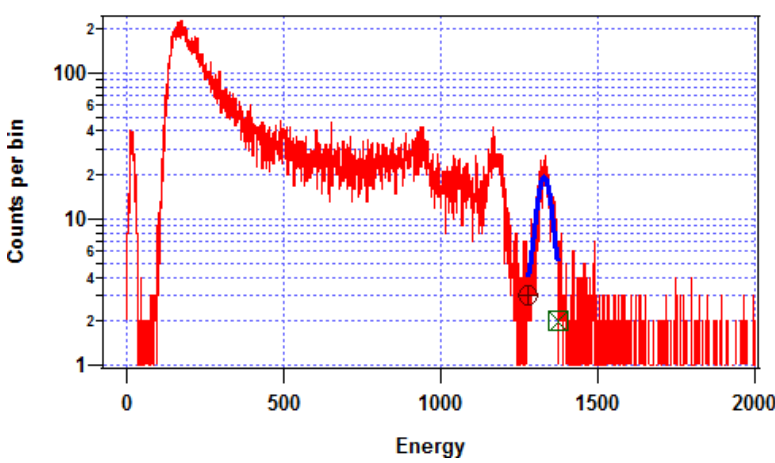
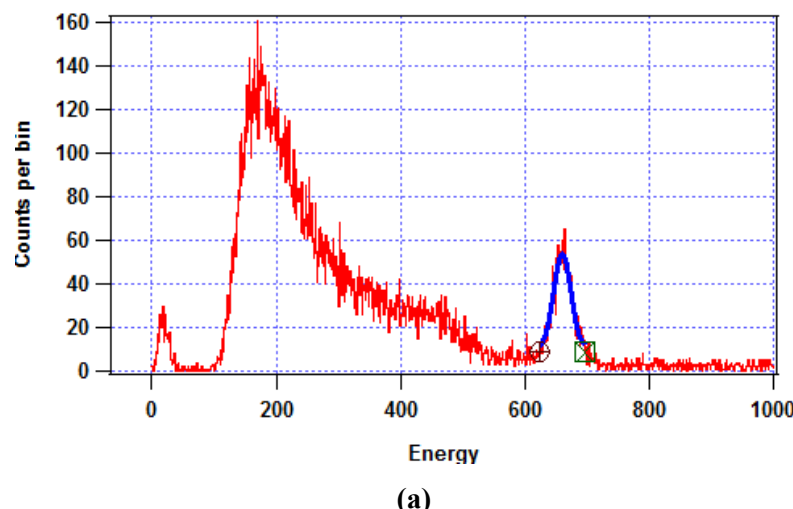
166 Experiments of pulse shape discrimination of neutrons and photons were performed exposing the CLYC6 cells
 167 to a beam emitted by a moderated $^{239}\text{PuBe}$ (α, n) source. Fig. 2a shows a PSD plot of RID versus energy, with the
 168 energy scale in keVee (electron equivalent) units calibrated using gamma sources. Neutron/photon separation is
 169 excellent on this plot. A figure of merit (FOM) was used to denote how well a CLYC6 detector can segregate
 170 neutrons from gamma rays via PSD. The PSD FOM of a detector was calculated as $FOM = T / (W_1 + W_2)$, where
 171 T is the distance between the centroids of the peaks of particle 1 (gamma rays) and particle 2 (thermal neutrons),
 172 W_1 is the FWHM of the peak of particle 1 and W_2 is the FWHM of the peak of particle 2 (see Fig. 2b). A FOM of
 173 2.3 was achieved for CLYC6 cells in this study. Particles are considered adequately separated with a $FOM \geq 1.27$
 174 [42]. Thus, the detected neutrons and gamma rays were successfully separated. The PSD technique can be utilized
 175 to perform simultaneous detection of both thermal neutrons and gamma rays using the developed detector system.
 176



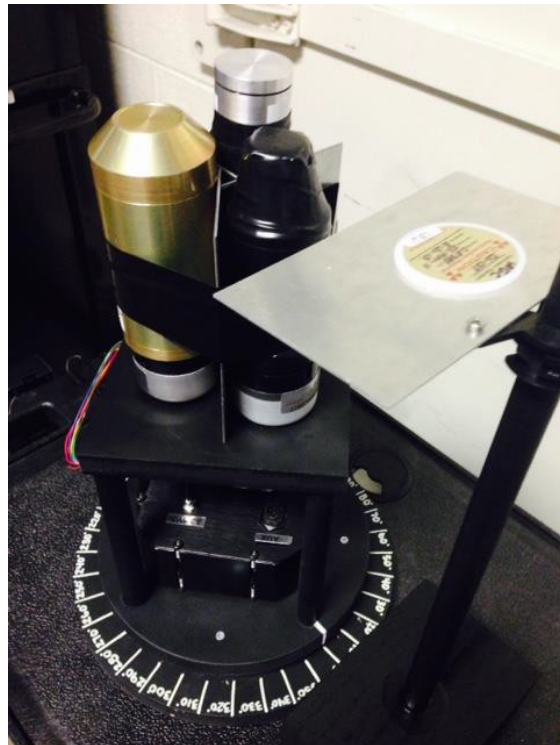
183 **Figure 2. (a)** Neutron/gamma PSD measurement for the CLYC cell using a moderated $^{239}\text{PuBe}$ source;
 184 **(b)** the neutron/gamma PSD FOM plot.

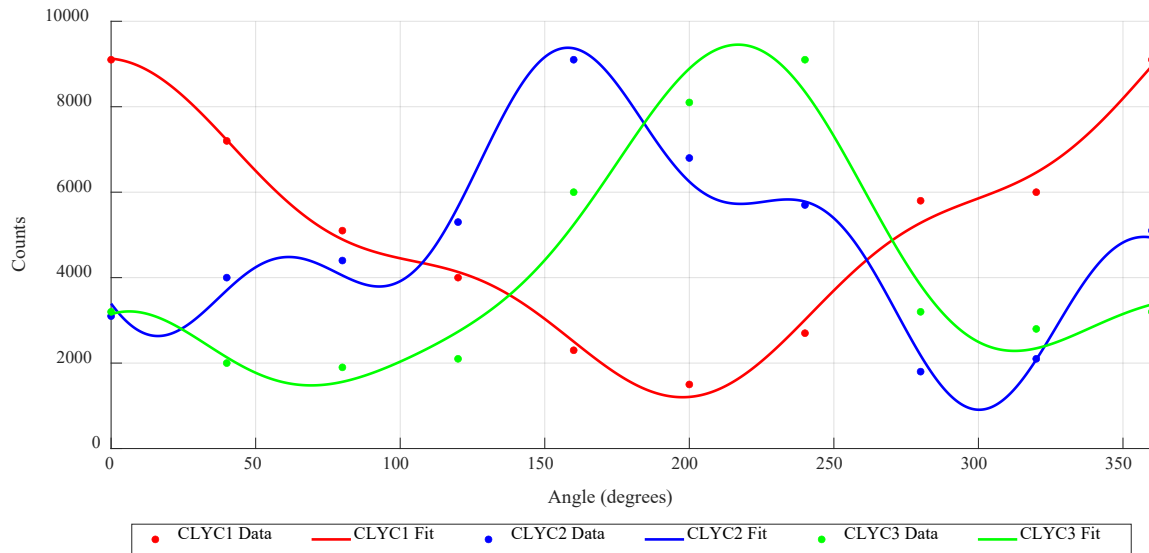
187
188 *3.2 Gamma spectroscopy*
189

190 The gamma-ray energy spectra of ^{137}Cs and ^{60}Co were recorded using photon data separated via PSD from
191 neutron data. The spectra for a 1-in diameter by 1-in height CLYC cell are shown in Fig. 3a,b. A Gaussian fit of
192 the ^{137}Cs peak at 662 keV (shown in blue) yields an energy resolution of 4.9% with approximately 1,496 counts
193 in the peak area. The Gaussian fit of the characteristic gamma-ray energy peak of 1.17 MeV for ^{60}Co yields an
194 energy resolution of 3.86% with approximately 816 counts. The Gaussian fit for the characteristic gamma-ray
195 energy peak of 1.33 MeV ^{60}Co yields an energy resolution of 3.6% with approximately 812 counts. The
196 measured resolution agrees with published data for CLYC elpasolites. Such energy resolution enables
197 spectroscopic analysis of gamma emitters and their quantification.
198
199

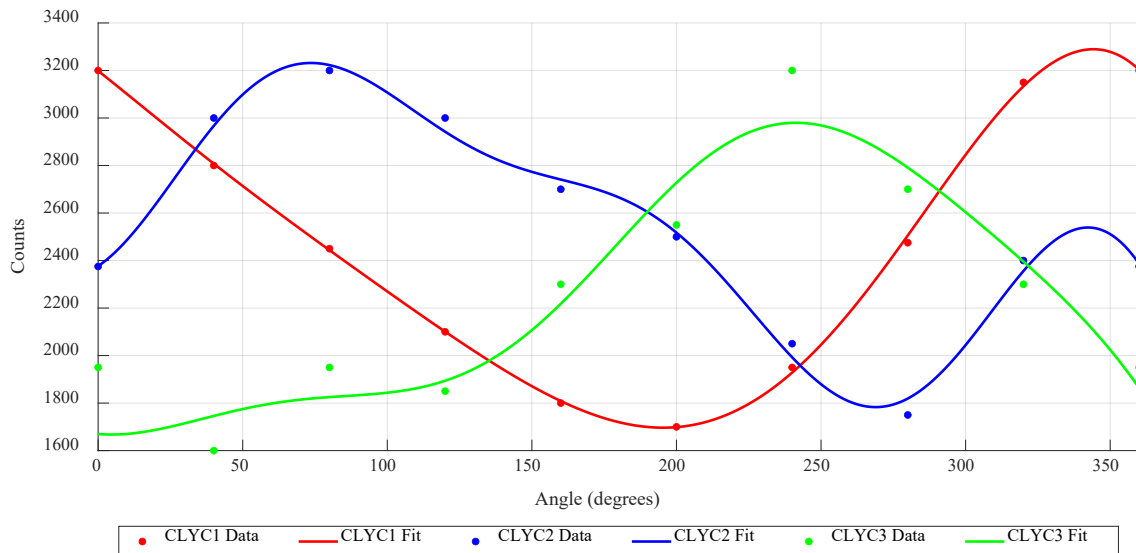


200
201 **Figure 3.** Gamma energy spectrum: (a) ^{137}Cs with Gaussian fit at the 662 keV peak and
202 (b) ^{60}Co 1.33 MeV peak.
203
204
205
206
207
208
209
210

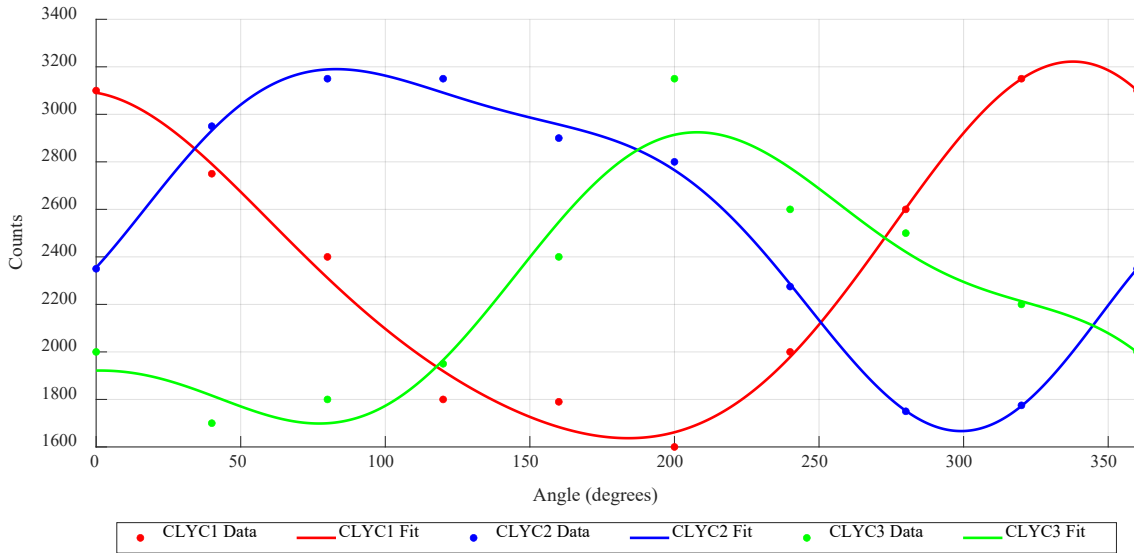
211 3.3 Source localization
212213 Directional measurements were carried out using the three-cell detector system with the ^{137}Cs and ^{60}Co gamma-ray sources and the $^{239}\text{PuBe}$ neutron source in various configurations. It should be noted that CLYC cell #1 is
214 centered with the 40° mark on the detector system turntable, CLYC #2 is centered with the 160° mark, and CLYC
215 #3 is centered with the 280° mark. Thus, 40° will be subtracted from the direction for which the maximum counts
216 occur for CLYC #1, 160° for CLYC #2, and 280° for CLYC #3 to obtain the inputs to the MLE algorithm.
217 Additionally, since the CLYC cell #3 contained a larger CLYC scintillator (1.5-inch diameter by 1.5-inch height),
218 all results for CLYC #3 were normalized to those of CLYC #1 and CLYC #2 so that the results would not be
219 skewed. The results of all configurations for the source localization measurements are summarized in Table 1.
220221 The first configuration was with the ^{137}Cs source placed in a plane $z = 0$ cm at the distance $R = 10$ cm from the
222 center of the detector system as shown in Fig. 4. The source was placed at the $0^\circ/360^\circ$ mark on the detector system
223 turntable. The results of directional measurements for this configuration are presented in Fig. 5a. The resulting
224 MLE evaluated direction to the source was 5° .
225226 The ^{137}Cs source was kept at the $0^\circ/360^\circ$ mark, but the distance from the center of the detector system and
227 height were varied. Measurements were performed for the following three configurations: (1) $R = 20$ cm and $z = 0$
228 cm, (2) $R = 10$ cm and $z = 10$ cm, and (3) $R = 20$ cm and $z = 10$ cm. The results for these three configurations are
229 presented in Fig. 5b,c,d, respectively. For $R = 20$ cm and $z = 0$ cm, the MLE source direction was $345^\circ \pm 2^\circ$. This
230 estimate deviated from the actual source direction by 15° . For source position at $R = 10$ cm and $z = 10$ cm, the
231 MLE source direction was $337^\circ \pm 16^\circ$. This deviated from the actual source direction by 23° . For $R = 20$ cm and z
232 = 10 cm, the MLE evaluation of the source direction was $6^\circ \pm 26^\circ$. This result deviated from the actual direction
by 6° .
233236 **Figure 4.** ^{137}Cs directional measurement.



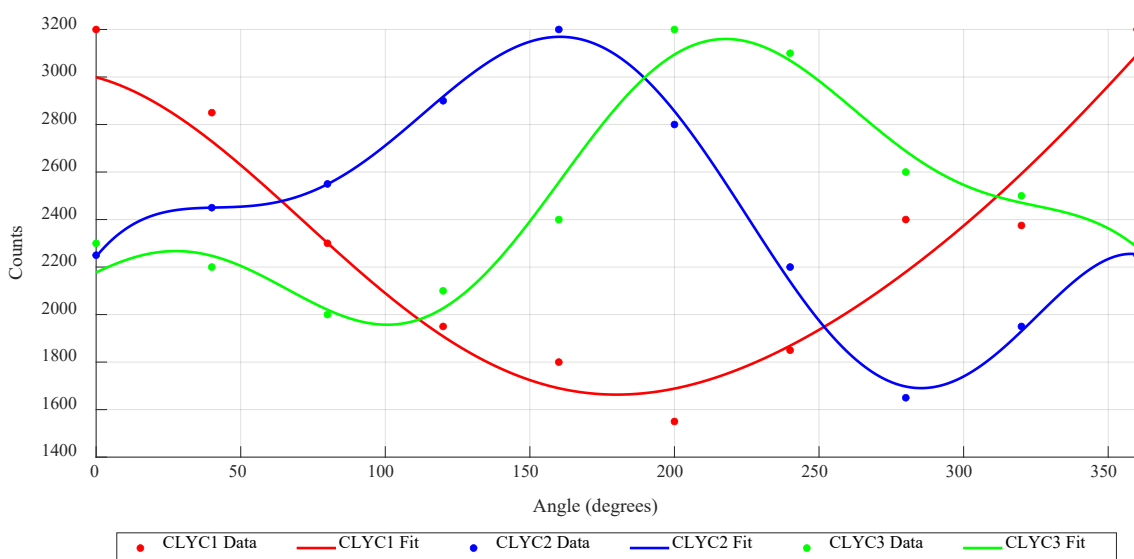
(a)



(b)



(c)



(d)

Figure 5. Directional measurement using a ^{137}Cs source placed at **(a)** $R = 10 \text{ cm}$, $z = 0 \text{ cm}$; **(b)** $R = 20 \text{ cm}$, $z = 0 \text{ cm}$; **(c)** $R = 10 \text{ cm}$, $z = 10 \text{ cm}$; **(d)** $R = 20 \text{ cm}$, $z = 10 \text{ cm}$.

259 A configuration consisting of both the ^{137}Cs and ^{60}Co gamma-ray sources was used as well. The ^{137}Cs source
260 was placed at the $0^\circ/360^\circ$ mark on the turntable in plane with the detector system ($z = 0$ cm) and at a distance of R
261 = 10 cm from the center of the system. The ^{60}Co source was placed at the 240° mark of the turntable 20 cm below
262 the plane of the detector system ($z = -20$ cm) and at $R = 10$ cm from the center of the directional detector. This setup
263 is shown in Fig. 6. The results for the ^{137}Cs source directional measurements are presented in Fig. 7a. The results
264 for the ^{60}Co source directional measurements are shown in Fig. 7b for the 1.17 MeV peak and Fig. 7c for the 1.33
265 MeV peak.

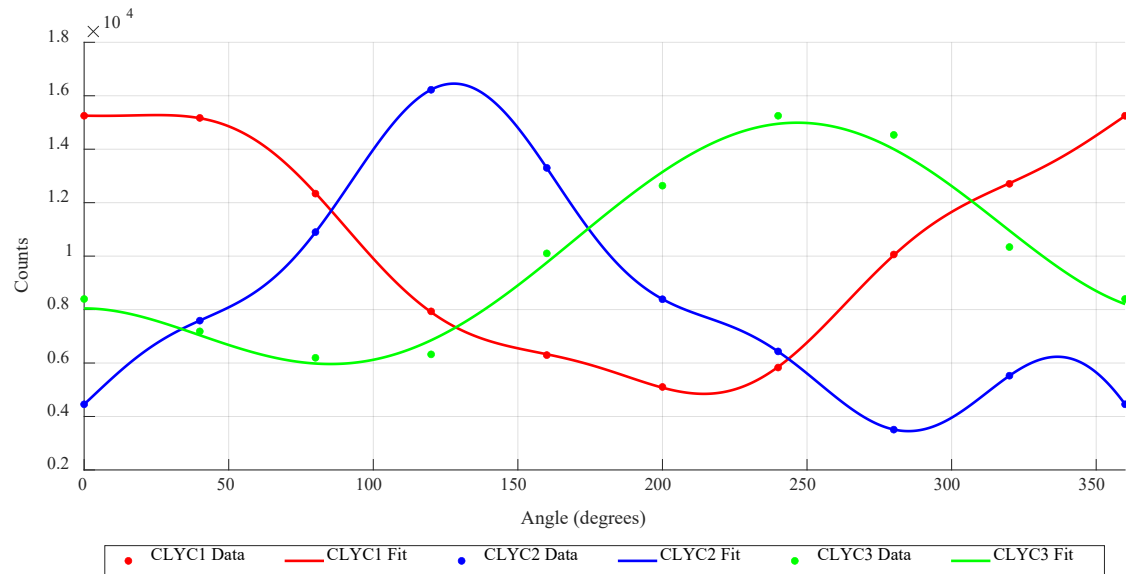
266
267



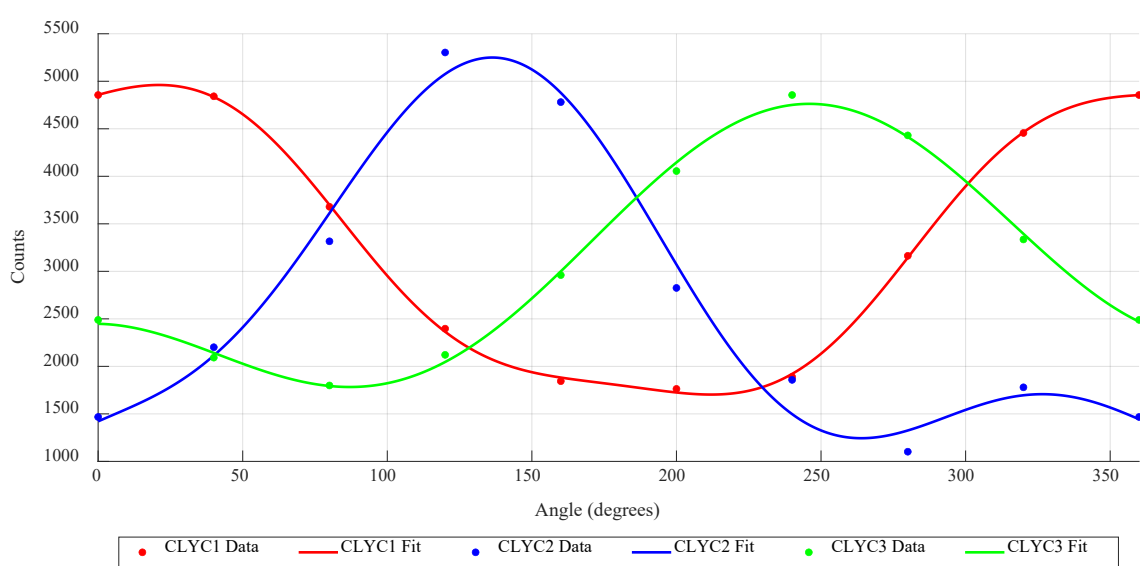
268
269

270 **Figure 6.** Two sources (^{137}Cs and ^{60}Co): directional measurement experimental setup.
271
272

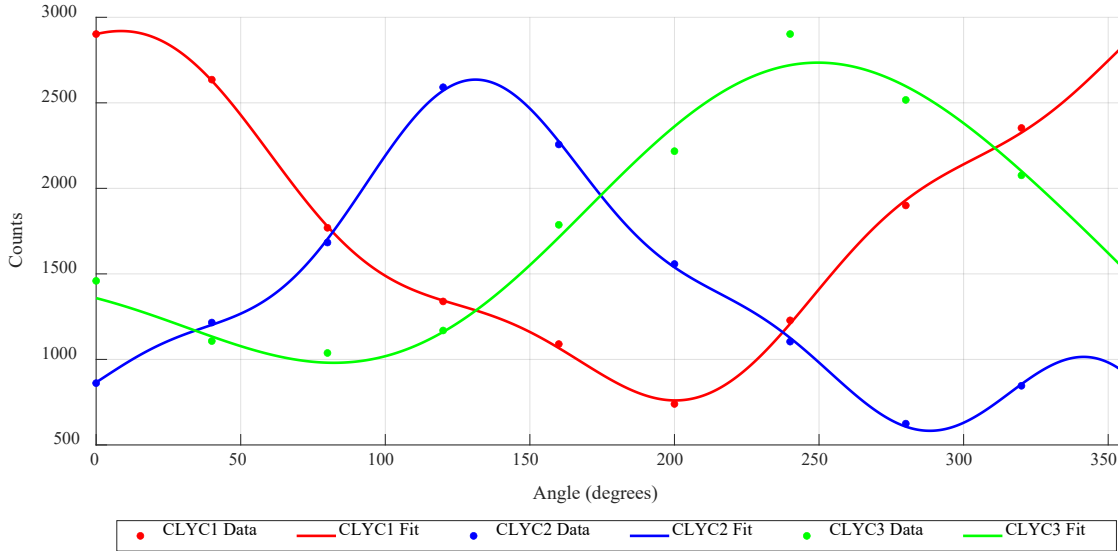
273 For the ^{137}Cs source, the MLE source direction was $13^\circ \pm 8^\circ$. This estimate deviated from the actual source
274 direction by 13° . For the ^{60}Co 1.17 MeV peak, the MLE source direction was $254^\circ \pm 6^\circ$. This deviated from the
275 actual source direction by 14° . For the ^{60}Co 1.33 MeV peak, the MLE source direction was $250^\circ \pm 1^\circ$. This deviated
276 from the actual source direction by 10° . The ^{60}Co source was also placed on top of the ^{137}Cs source to determine the
277 feasibility of detecting two collocated gamma sources. The MLE estimates of the source direction for both sources
278 agreed with the actual source direction of $0^\circ/360^\circ$.
279
280



(a)



(b)



286
287 (c)
288

289 **Figure 7.** Two-source directional measurement results for (a) ^{137}Cs 662 keV peak; (b) ^{60}Co 1.17 MeV peak; (c)
290 ^{60}Co 1.33 MeV peak.

291
292
293 Two locations for the $^{239}\text{PuBe}$ source were used in directional measurements. The source was placed at the
294 0°/360° mark on the detector system turntable in-plane with the detector system ($z = 0$ m) and at 1 m from the center
295 of the system. This setup is shown in Fig. 8. The measurement results for this configuration are shown in Fig. 9a.
296 The MLE evaluation of the source direction was $359^\circ \pm 36^\circ$; a difference of 1° from the actual source direction.

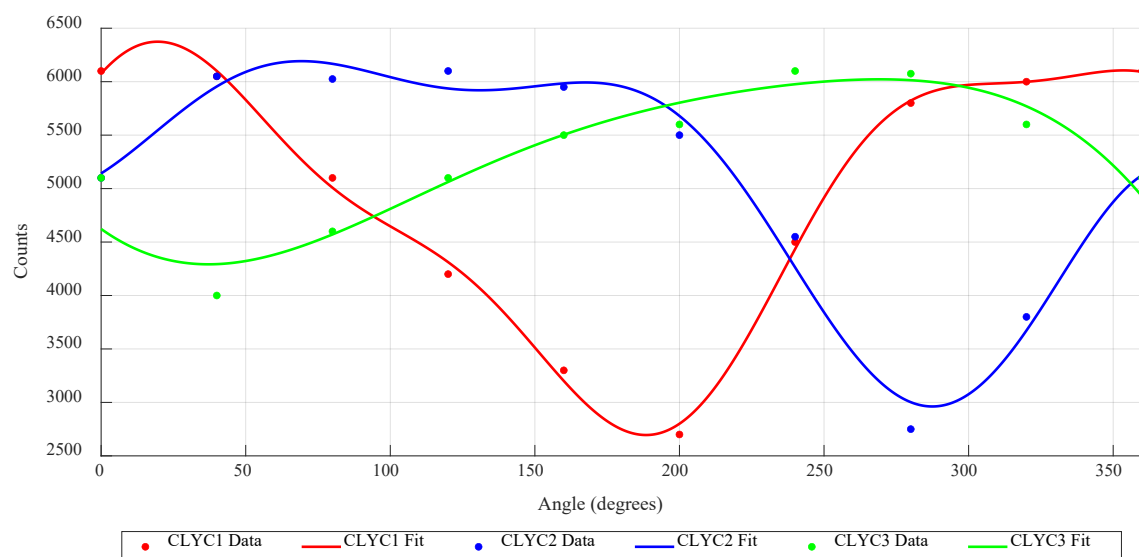
297 The source was then moved out to $R = 3$ m from the center of the detector system and remained at a height in-
298 plane with the detector system. The results for this source-detector arrangement are presented in Fig. 9b. The MLE
299 source direction was $19^\circ \pm 6^\circ$. This deviated from the actual source direction by 19° .

300 It is hypothesized that the discrepancies observed in source direction can be eliminated by increasing the
301 measurement time at each angle and increasing the angle increments at which measurements are performed (i.e.,
302 collect measurements at every 10° instead of 40°). These discrepancies can also be addressed by utilizing a
303 directional detection system of identical CLYC cells of the same size and quality, identical PMTs and identical
304 aluminum housings. In this study, two of the three CLYC detectors used in the three-cell system were the same
305 size. In the directional neutron measurements, the shielded vault caused neutron scattering from concrete walls and
306 the floor. The beam port of the shielded container of the $^{239}\text{PuBe}$ source generated a wide beam of low energy
307 neutrons, thus resulting in the wide angular distribution of neutron emission towards the directional detector. In
308 field measurements at longer distances, this ‘room’ effect will be less important.

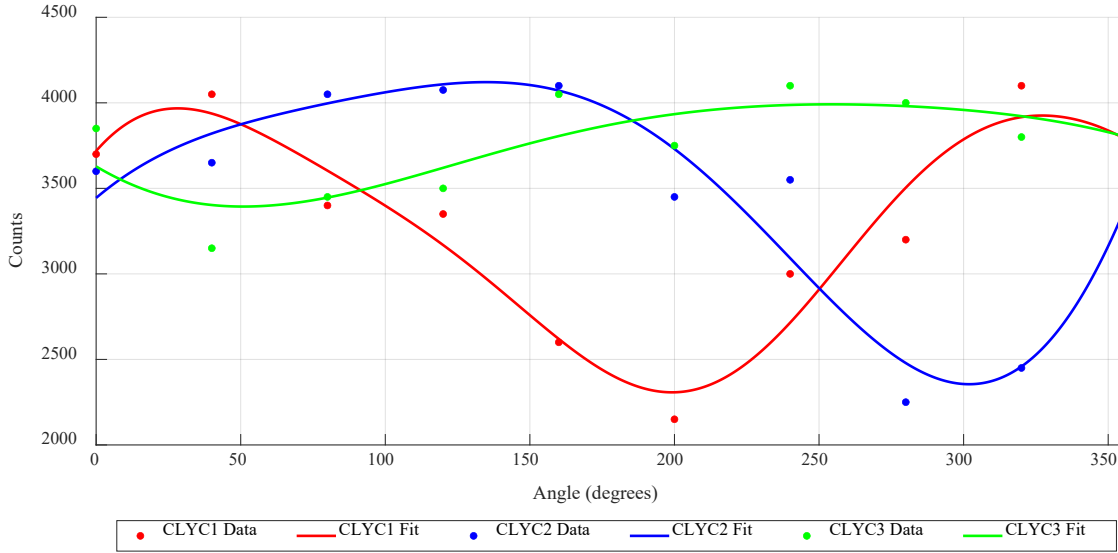
309
310



311
312
313 **Figure 8.** Directional measurements using a moderated $^{239}\text{PuBe}$ source.
314
315



316
317 (a)



318
319 **(b)**
320
321 **Figure 9.** $^{239}\text{PuBe}$ directional measurement results: **(a)** $R = 1$ m, $z = 0$ m; **(b)** $R = 3$ m, $z = 0$ m.
322
323
324
325

Table 1
MLE estimates of angle pointing to the source.

Source Type	Source Location	Actual Source Angle	MLE Source Angle $\pm \sigma$	Actual vs MLE Angle Difference
^{137}Cs	$R = 10$ cm, $z = 0$ cm	$0^\circ/360^\circ$	$5^\circ \pm 25^\circ$	5°
^{137}Cs	$R = 20$ cm, $z = 0$ cm	$0^\circ/360^\circ$	$345^\circ \pm 2^\circ$	15°
^{137}Cs	$R = 10$ cm, $z = 10$ cm	$0^\circ/360^\circ$	$337^\circ \pm 16^\circ$	23°
^{137}Cs	$R = 20$ cm, $z = 10$ cm	$0^\circ/360^\circ$	$6^\circ \pm 26^\circ$	6°
$^{137}\text{Cs} + ^{60}\text{Co}$ (^{137}Cs 662 keV used)	$R = 10$ cm, $z = 0$ cm	$0^\circ/360^\circ$	$13^\circ \pm 8^\circ$	13°
$^{137}\text{Cs} + ^{60}\text{Co}$ (^{60}Co 1.17 MeV used)	$R = 10$ cm, $z = -20$ cm	240°	$254^\circ \pm 6^\circ$	14°
$^{137}\text{Cs} + ^{60}\text{Co}$ (^{60}Co 1.33 MeV used)	$R = 10$ cm, $z = -20$ cm	240°	$250^\circ \pm 1^\circ$	10°
$^{239}\text{PuBe}$	$R = 1$ m, $z = 0$ m	$0^\circ/360^\circ$	$359^\circ \pm 36^\circ$	1°
$^{239}\text{PuBe}$	$R = 3$ m, $z = 0$ m	$0^\circ/360^\circ$	$19^\circ \pm 6^\circ$	19°

4. Conclusion

326
327 A detector system consisting of an array of CLYC-based detectors was studied for directional, simultaneous
328 thermal neutron and gamma-ray measurements. The detector system was tested using a single ^{137}Cs photon source,
329 two gamma sources simultaneously (^{137}Cs and ^{60}Co), and a moderated $^{239}\text{PuBe}$ source in various configurations.
330 Directional measurements were carried out through 360° rotation in increments of 40° . The MLE algorithm was
331 used to estimate the most probable direction to the source based on counts measured in each of the three elpasolite
332 cells. The evaluation of the cell's responses showed that the three-cell array is feasible to determine the direction
333 to a point-like gamma-ray source and thermal neutron source simultaneously.
334

335 For most configurations, the direction to a source was estimated within the standard deviation. The maximum
336 error (actual versus MLE) of the discrepant results was 23° . This error can be reduced by increasing time of
337 measurement and increasing the number of increments to be measured in 360° . The error can also be reduced by
338

339 homogenizing the detector system (i.e., same size/quality CLYC cells, same PMTs, same housings). The
340 directional measurements using the system for search of point neutron sources at longer distances in the field will
341 demonstrate reduced error of the angle evaluation.

342 This three-CLYC detector system with the MLE enabled source localization would allow an end-user to search
343 for missing/stolen radiological or nuclear materials, WMDs and RDDs, with improved direction estimates at each
344 step while approaching the source. This system could also be used in a variety of other applications including
345 environmental safety and waste management.

346 347 Acknowledgments

348
349 This manuscript has been authored by Mission Support and Test Services, LLC, under Contract No. DE-
350 NA0003624 with the U.S. Department of Energy and supported by the Site-Directed Research and Development
351 Program, NA USDOE National Nuclear Security Administration (NNSA). The United States Government retains
352 and the publisher, by accepting the article for publication, acknowledges that the United States Government retains
353 a non-exclusive, paid-up, irrevocable, worldwide license to publish or reproduce the published form of this
354 manuscript, or allow others to do so, for United States Government purposes. The U.S. Department of Energy will
355 provide public access to these results of federally sponsored research in accordance with the DOE Public Access
356 Plan (<http://energy.gov/downloads/doe-public-access-plan>). The views expressed in the article do not necessarily
357 represent the views of the U.S. Department of Energy or the United States Government. DOE/NV/03624--0853.

358 The authors acknowledge the professional staff of RMD, Watertown, Massachusetts, for the production of the
359 scintillators, for providing these detectors to the Remote Sensing Laboratory, and for their support and advice.

360 361 References

- 362 [1] J. Doyle, Nuclear Safeguards, Security and Nonproliferation, Elsevier, Oxford, UK, 2008.
- 363 [2] R. Runkle, Neutron sensors and their role in nuclear nonproliferation, Nuclear Instruments and Methods in
364 Physics Research A, 652 (2011) 37-40.
- 365 [3] D.M. Trombetta, M. Klintefjord, K. Axell, B. Cederwall, Fast neutron- and γ -ray coincidence detection for
366 nuclear security and safeguards applications. Nuclear Instruments and Methods in Physics Research A, 927 (2019)
367 119-124.
- 368 [4] J. Hite, J. Mattingly, D. Archer, M. Willis, A. Rowe, K. Bray, J. Carter, J. Ghawaly, Localization of a radioactive
369 source in an urban environment using Bayesian Metropolis methods. Nuclear Instruments and Methods in Physics
370 Research A, 915 (2019) 82-93.
- 371 [5] K. Moody, P. Grant, I. Hutcheon, Y. Varoufakis, Nuclear Forensic Analysis, Taylor & Francis, New York, NY,
372 2014.
- 373 [6] International Atomic Energy Agency (IAEA), Sealed Radioactive Sources, Oct 2013, available at
374 <https://www.iaea.org/sites/default/files/sealedradsources1013.pdf> (accessed on June 29, 2020).
- 375 [7] G. Steinhauser, A. Brandl, T. Johnson, Comparison of the Chernobyl and Fukushima nuclear accidents: a review
376 of the environmental impacts. Science of the Total Environment, 471 (2014) 800-817.
- 377 [8] Y. Sanada, T. Torii, Aerial radiation monitoring around the Fukushima Daiichi Nuclear Power Plant using an
378 unmanned helicopter. Journal of Environmental Radioactivity, 139 (2015) 294-299.
- 379 [9] W. Barletta, The Fukushima Dai-ichi accident and its implications for the safety of nuclear power. Nuclear
380 Instruments and Methods in Physics Research A, 817 (2016) A1-A3.
- 381 [10] T. Kurihara, K. Tanada, J. Kataoka, H. Hosokoshi, S. Mochizuki, L. Tagawa, H. Okochi, Y. Gotoh, Precision
382 spectroscopy of cesium-137 from the ground to 150 m above in Fukushima. Nuclear Instruments and Methods in
383 Physics Research A, 978 (2020) 164414.

384 [11] N.E. Stauff, T.K. Kim, T.A. Taiwo, Variations in nuclear waste management performance of various fuel-
385 cycle options. *Journal of Nuclear Science and Technology*, 52 (2015) 1058-1073.

386 [12] M. Greenberg, K. Lowrie, J. Burger, C. Powers, M. Gochfeld, H. Mayer, Preferences for alternative risk
387 management policies at the United States major nuclear weapons legacy sites. *Journal of Environmental Planning
388 and Management*, 50(2) (2007) 187-209.

389 [13] D.L. Chichester, J.D. Simpson, M. Lemchak, Advanced compact accelerator neutron generator technology for
390 active neutron interrogation field work. *Journal of Radioanalytical and Nuclear Chemistry*, 271 (2007) 629-637.

391 [14] A. Barzilov, P. Womble, Study of Doppler broadening of gamma-ray spectra in 14-MeV neutron activation
392 analysis. *Journal of Radioanalytical and Nuclear Chemistry*, 301 (2014) 811-819.

393 [15] J. Bendahan, Review of active interrogation techniques. *Nuclear Instruments and Methods in Physics Research
394 A*, 954 (2020) 161120.

395 [16] A. Poitrasson-Rivière, J.K. Polack, M.C. Hamel, D.D. Klemm, K. Ito, A.T. McSpaden, M. Flaska, S.D. Clarke,
396 S.A. Pozzi, A. Tomanin, P. Peerani, Angular-resolution and material-characterization measurements for a dual-
397 particle imaging system with mixed-oxide fuel. *Nuclear Instruments and Methods in Physics Research A*, 797
398 (2015) 278-284.

399 [17] J. Hartman, A. Pour Yazdanpanah, A. Barzilov, E. Regentova, 3D imaging using combined neutron-photon
400 fan-beam tomography: A Monte Carlo study. *Applied Radiation and Isotopes*, 111 (2016) 110-116.

401 [18] G.F. Knoll, *Radiation Detection and Measurement*, 4th ed., Wiley, New York, 2010.

402 [19] N. Zaitseva, B. Rupert, I. Pawelczak, A. Glenn, H.P. Martinez, L. Carman, M. Faust, N. Cherepy, S. Payne,
403 Plastic scintillators with efficient neutron/gamma pulse shape discrimination. *Nuclear Instruments and Methods in
404 Physics Research A*, 668 (2012) 88-93.

405 [20] D. Cester, G. Nebbia, L. Stevanato, F. Pino, G. Viesti, Experimental tests of the new plastic scintillator with
406 pulse shape discrimination capabilities EJ-299-33. *Nuclear Instruments and Methods in Physics Research A*, 735
407 (2014) 202-206.

408 [21] J. Qin, C. Lai, B. Ye, R. Liu, X. Zhang, L. Jiang, Characterizations of BC501A and BC537 liquid scintillator
409 detectors. *Applied Radiation and Isotopes*, 104 (2015) 15-24.

410 [22] K. Biswas, M.H. Du, Energy transport and scintillation of cerium-doped elpasolite $\text{Cs}_2\text{LiYCl}_6$: hybrid density
411 functional calculations. *Physical Review B*, 86 (2012) 014102.

412 [23] J. Glodo, R. Hawrami, K.S. Shah, Development of $\text{Cs}_2\text{LiYCl}_6$ scintillator. *Journal of Crystal Growth*, 379
413 (2013) 73-78.

414 [24] R. Machrafi, N. Khan, A. Miller, Response functions of $\text{Cs}_2\text{LiYCl}_6:\text{Ce}$ scintillator to neutron and gamma
415 radiation. *Radiation Measurements* 70 (2014) 5-10.

416 [25] N. D'Olympia, P. Chowdhury, C.J. Guess, T. Harrington, E.G. Jackson, S. Lakshmi, C.J. Lister, J. Glodo, R.
417 Hawrami, K.S. Shah, U. Shirwadkar, Optimizing $\text{Cs}_2\text{LiYCl}_6$ for fast neutron spectroscopy. *Nuclear Instruments and
418 Methods in Physics Research A*, 694 (2012) 140-146.

419 [26] M.B. Smith, T. Achtzehn, H.R. Andres, E.T.H. Clifford, P. Forget, J. Glodo, R. Hawrami, H. Ing, P.
420 O'Doughtery, K.S. Shah, U. Shirwadkar, L. Soundara-Pandian, J. Tower, Fast neutron measurements using
421 $\text{Cs}_2\text{LiYCl}_6:\text{Ce}$ (CLYC) scintillator, *Nuclear Instruments and Methods in Physics Research A*, 784 (2015) 162-167.

422 [27] E.V.D. Van Loef, P. Dorenbos, C.W.E. Van Eijk, K.W. Krämer, H.U. Güdel, Scintillation and spectroscopy
423 of the pure and Ce^{3+} -doped elpasolites: Cs_2LiYX_6 ($X = \text{Cl}; \text{Br}$). *Journal of Physics: Condensed Matter*, 14 (2002)
424 8481-8496.

425 [28] J. Glodo, E. Van Loef, R. Hawrami, W.M. Higgins, A. Churilov, U. Shirwadkar, K.S. Shah, Selected properties
426 of $\text{Cs}_2\text{LiYCl}_6$, $\text{Cs}_2\text{LiLaCl}_6$, and $\text{Cs}_2\text{LiLaBr}_6$ scintillators. *IEEE Transactions on Nuclear Science*, 58 (2011) 333-338.

427 [29] P. Rodnyi, Core-valence luminescence in scintillators. *Radiation Measurements*, 38 (2004) 343-352.

428 [30] N. D'Olympia, P. Chowdhury, C.J. Lister, J. Glodo, R. Hawrami, K. Shah, U. Shirwadkar, Pulse-shape analysis
429 of CLYC for thermal neutrons, fast neutrons, and gamma-rays. *Nuclear Instruments and Methods in Physics*
430 *Research A*, 714 (2013) 121-127.

431 [31] A. Giaz, L. Pellegrini, F. Camera, N. Blasi, S. Brambilla, S. Ceruti, B. Million, S. Riboldi, C. Cazzaniga, G.
432 Gorini, M. Nocente, A. Pietropaolo, M. Pillon, M. Rebai, M. Tardocchi, The CLYC-6 and CLYC-7 response to
433 gamma-rays, fast and thermal neutrons. *Nuclear Instruments and Methods in Physics Research A*, 810 (2016) 132-
434 139.

435 [32] Radiation Monitoring Devices, Gamma-Neutron Scintillator Properties - CLYC, available at
436 <https://www.dynasil.com/assets/CLYC-Gamma-Neutron-Scintillator-Properties.pdf> (accessed on June 29, 2020).

437 [33] C.M. Bartle, G.V.M. Williams, An efficient directional fast neutron sensor for a mixed radiation field. *Rad.*
438 *Meas.*, 46 (2011) 1716-1719.

439 [34] A. Weltz, B. Torres, L. McElwain, R. Dahal, J. Huang, I. Bhat, J. Lu, Y. Danon, Development of a modular
440 directional and spectral neutron detection system using solid-state detectors. *Nuclear Instruments and Methods in*
441 *Physics Research A*, 792 (2015) 28-37.

442 [35] Y. Fu, Y. Tian, Y. Li, J. Yang, J. Li, Directional fast neutron detection using a time projection chamber and
443 plastic scintillation detectors. *Nuclear Instruments and Methods in Physics Research A*, 954 (2020) 161445.

444 [36] Y. Sato, K. Minemoto, M. Nemoto, T. Torii, Construction of virtual reality system for radiation working
445 environment reproduced by gamma-ray imagers combined with SLAM technologies. *Nuclear Instruments and*
446 *Methods in Physics Research A*, 976 (2020) 164286.

447 [37] D. Goodman, J. Xia, Z. He, Qualitative measurement of spatial shielding isotopes via Compton imaging
448 neutron-induced gamma rays using 3-D CdZnTe detectors. *Nuclear Instruments and Methods in Physics Research*
449 *A*, 935 (2019) 214-221.

450 [38] P. Guss, S. Mukhopadhyay, Dual gamma neutron directional elpasolite detector, in: *SPIE Proc.* 8854 (2013)
451 885402.

452 [39] P. Guss, T. Stampahar, S. Mukhopadhyay, J. Lee, K. Shah, M. Squillante, W. Higgins, Novel deployment of
453 elpasolites as a dual gamma-neutron directional detector, in: *Site Directed Research & Development, Remote*
454 *Sensing Laboratory-Nellis*, 2013.

455 [40] A. Guckes, A. Barzilov, P. Guss, Directional detection of neutrons and photons using elpasolites:
456 computational study, *Radiations Measurements*, 124 (2019) 127 - 131.

457 [41] S.R. Eliason, Maximum likelihood estimation, Sage Publications, Newbury Park, CA, 1993.

458 [42] A. Lintereur, J. Ely, J. Stave, B. Macdonald, Neutron and gamma ray pulse shape discrimination with
459 polyvinyltoluene, PNNL-21609, Pacific Northwest National Laboratory, Mar 2012, available at
460 https://www.pnnl.gov/main/publications/external/technical_reports/PNNL-21609.pdf (accessed on June 29,
461 2020).